

Measurement of Absolute Myocardial Blood Flow With H₂¹⁵O and Dynamic Positron-Emission Tomography

Strategy for Quantification in Relation to the Partial-Volume Effect

Hidehiro Iida, DSc, Iwao Kanno, PhD, Akira Takahashi, MD, Shuichi Miura, PhD, Matsutaro Murakami, PhD, Kazuhiro Takahashi, MS, Yukihiko Ono, MD, Fumio Shishido, MD, Atsushi Inugami, MD, Noriaki Tomura, MD, Shuichi Higano, MD, Hideaki Fujita, MD, Hiroshi Sasaki, BS, Hiroyuki Nakamichi, BS, Shigenori Mizusawa, BS, Yasushi Kondo, BS, and Kazuo Uemura, MD

An in vivo technique was developed for measuring the absolute myocardial blood flow with H₂¹⁵O and dynamic positron-emission tomography. This technique was based on a new model involving the concept of the tissue fraction, which was defined as the fraction of the tissue mass in the volume of the region of interest. The myocardium was imaged dynamically by positron-emission tomography, starting at the time of intravenous bolus injection of H₂¹⁵O. The arterial input function was measured continuously with a beta-ray detector. A separate image after C¹⁵O inhalation was also obtained for correction of the H₂¹⁵O radioactivity in the blood. The absolute myocardial blood flow and the tissue fraction were calculated for 15 subjects with a kinetic technique under region-of-interest analysis. These results seem consistent with their coronary angiographic findings. The mean value of the measured absolute myocardial blood flows in normal subjects was 0.95 ± 0.09 ml/min/g. This technique detected a diffuse decrease of myocardial blood flow in patients with triple-vessel disease. (*Circulation* 1988;78:104–115)

With the use of suitable tracers and appropriate mathematical models, positron-emission tomography (PET) has the capability of providing noninvasive quantitative measurements of physiological functions in organs. However, in the field of cardiac PET, relatively few measurements have been made of the absolute value of the myocardial blood flow (MBF) and metabolism.^{1,2} The main reason for this concerns the so-called partial volume effect (PVE),^{1–6} that is, the spillover effect in radioactivity measurement due to the relatively thin-walled myocardium compared with the spatial resolution of PET,⁷ and the wall motion of the myocardium. The PVE problem

might be resolved if the myocardium could be imaged with an infinitely high-resolution PET scanner with an electrocardiographic gating scan. This is, however, still impractical. In the present study, we developed an alternative approach based on kinetic analysis.

Performing kinetic analysis for dynamic measurements, in general, allows two or more parameter determinations to be made. For example, single-compartment kinetic analysis for a diffusible tracer gives the regional blood flow and the tracer distribution volume in units per space. The distribution volume obtained here is related to the tissue/blood partition coefficient of the tracer and the tissue fraction in the region to be analyzed. In the present study, to exclude the effect of the PVE when analyzing PET data, we developed a modified single-compartment model that included the concept of the tissue fraction. The tissue fraction can be determined from this type of kinetic model analysis, assuming that the tissue/blood partition coefficient can be fixed.

From the Department of Radiology and Nuclear Medicine, Department of Internal Medicine (A.T., Y.O., H.N., S.M.), and Department of Neurology (Y.K.), Research Institute for Brain and Blood Vessels-AKITA, Akita City, Akita, Japan.

Address for correspondence: Hidehiro Iida, DSc, Department of Radiology and Nuclear Medicine, Research Institute for Brain and Blood Vessels-AKITA, 6-10 Senshu-Kubota-machi, Akita City, Akita 010, Japan.

Received March 31, 1987; revision accepted March 17, 1988.

¹⁵O-Labeled water (H₂¹⁵O) was used as the tracer in this study because it has the following advantages. The tissue/blood partition coefficient of water is almost the same in each individual, and the distribution is almost uniform in the myocardium. Kety's model^{8,9} is applicable because H₂¹⁵O is chemically inert and diffusible. The measurement is repeatable because of the short half-life of ¹⁵O (123 seconds). In practice, H₂¹⁵O is easier to handle compared with other diffusible tracers such as inert gases.

Based on the use of H₂¹⁵O and dynamic PET, the present study outlines our new approach for overcoming the PVE in cardiac PET studies. Quantitative absolute measurements of MBF were obtained in 15 subjects. A conventional H₂¹⁵O autoradiographic method was also examined together with its limitations for quantification.

Subjects and Methods

Model Description

The theory for the measurement of MBF is based on the principle of inert gas exchange developed by Kety,^{8,9} except that the present model includes the concept of the tissue fraction, α (g/ml), as illustrated in Figure 1; α is defined as the ratio of the tissue mass, W (g), to the volume of the region of interest (ROI), V (ml):

$$\alpha = W/V \quad (1)$$

By assuming a uniform and constant flow, F (ml/min), and instantaneous equilibrium, the tracer balance in the ROI can be expressed by

$$\frac{dQ(t)}{dt} = EF Ca(t) - \frac{EF}{p} Cm(t) \quad (2)$$

where Q(t) (μ Ci) is the total tracer amount in the ROI, E is the extraction fraction, p (ml/g) is the tissue/blood partition coefficient, Ca(t) (μ Ci/ml) is the tracer artery concentration, and Cm(t) (μ Ci) is the net tissue concentration. Note that Cm(t) is not

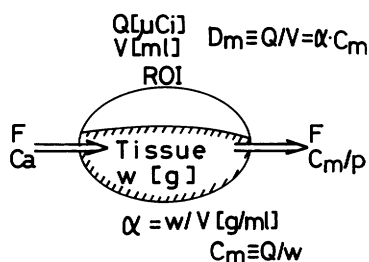


FIGURE 1. Schematic model for measurement of the absolute myocardial blood flow. A small region-of-interest (ROI) element of volume, V (ml) has a tissue mass of W (g). W/V ratio is the tissue fraction, α (g/ml). ROI element is perfused with a blood flow, F (ml/min), which transports tracer of concentration, Ca(t), to the tissue element. Tracer is well mixed in the tissue. ROI concentration, Dm(t), and the tissue concentration, Cm(t), are related by: Dm(t)= α Cm(t).

observable and is related to the measured ROI concentration, Dm(t), by

$$Dm(t) = \alpha Cm(t) \quad (3)$$

Dividing Equation 2 by V, and incorporating Equations 1 and 3, we have

$$\frac{dDm(t)}{dt} = \alpha Ef Ca(t) - \frac{Ef}{p} Dm(t) \quad (4)$$

where f is the regional blood flow defined by

$$f = F/V \quad (5)$$

Note that Equation 4 represents the relation between two observed variables [Dm(t) and Ca(t)] and two model parameters (f and α) when E and p are given. It should also be mentioned that the obtained f is free from PVE; that is, F and V are free from PVE. PVE is already included in α . Solving Equation 4 for Dm(t) gives

$$Dm(t) = \alpha Ef Ca(t) * \exp(-Ef/p t) \\ = k_1 Ca(t) * \exp(-k_2 t) \quad (6)$$

where Dm(t=0)=0 is assumed, and the asterisk is the convolution integral.

Two parameters in Equation 6, k_1 ($=\alpha Ef$) and k_2 ($=Ef/p$), are determined simultaneously so that the calculated tissue curve reproduces the measured dynamic data best by means of the least-squares fitting (χ^2 minimizing) technique (see below). Therefore, MBF (free from PVE), f, and α are obtained from $f=k_2 \cdot p/E$ and $\alpha=(k_1/k_2)/p$, respectively, based on the assumptions that p and E can be fixed ($p=0.91$ ml/g and $E=1$). The value of p is determined as the ratio of the water content in the myocardium (0.78 g water/g tissue)¹⁰ to that in the blood (0.86 g water/ml blood for a hematocrit of about 0.45).¹⁰⁻¹² The validity of these assumptions will be examined later (see "Discussion").

Myocardial Blood Flow Imaging by the Autoradiographic Method

When measuring the cerebral blood flow by the conventional autoradiographic method,¹³⁻¹⁷ it is necessary to fix the value of the tissue fraction (commonly as $\alpha=1$ g/ml). Integrating both sides of Equation 6 for the time duration ($t_1=0$, t_2) gives

$$\int_{t_1}^{t_2} Dm(t) dt = \alpha Ef \int_{t_1}^{t_2} Ca(t) * \exp(-Ef/p t) dt \quad (7)$$

The right side of Equation 7 can be calculated with the measured artery concentration curve, Ca(t), for various Ef values, that is, from 0.01 to 2 ml/min/g in 0.01 steps. Here, the tissue fraction is fixed as $\alpha=1$ g/ml.⁴⁻⁶ Therefore, we can obtain the relation between the Ef value and the PET scan data, $\int_{t_1}^{t_2} Dm(t) dt$. Once the right side of Equation 7 has been calculated, a unique f value can be determined for each pixel of the tomographic image data by the

look-up-table procedure. Here, the tissue/blood partition coefficient is fixed as $p=0.91 \text{ ml/g}$.

Subjects

The present study was performed on seven normal subjects and eight patients. The normal subjects consisted of two groups. One included four normal volunteers (N1–N4), and the other included three subnormal subjects (S1–S3) who were suspected of angina pectoris because of complaints of chest pain, but had normal coronary angiographic findings (see "Results"). Three of the patients (P1, P2, and P6) were diagnosed as having angina pectoris, and the other five (P3–P5, P7, and P8) were diagnosed as having myocardial infarction. Diagnosis, interval from onset to PET, and the interval from coronary angiography to PET are listed in Table 1.

For all subnormal subjects and patients, conventional coronary angiography was performed before the PET study. The angiographic data were interpreted by angiographers who were test blinded with respect to the PET data.

Production of H_2^{15}O

H_2^{15}O was synthesized by an in-target direct method.¹⁸ The target gas (3.5 kg/cm^2 of $0.1\% \text{ H}_2$ in N_2) was bombarded by 6.8 MeV deuterons. ^{15}O was produced by the reaction of $^{14}\text{N}(\text{d},\text{n})^{15}\text{O}$, and H_2^{15}O vapor was produced by $2\text{H}_2 + ^{15}\text{O}_2 \rightarrow 2\text{H}_2^{15}\text{O}$. The resultant H_2^{15}O vapor was channeled directly to an automatic injection unit in the PET room and trapped by bubbling into a 5-ml saline-filled vial.

PET Scanner

The PET scanner was a HEADTOME-III¹⁹ installed at our institute, a three-ring and five-slice machine. The standard-resolution collimator was used. In the H_2^{15}O study, a high-speed mode was selected to achieve quick data acquisition, which

took 2.5 seconds for a single complete data acquisition while making continuous motions of the wobble and rotation of the detector ring.

In the present study, images were taken with intervals of 5 or 15 seconds as described below. Data were reconstructed with $2 \times 2\text{-mm}^2$ pixel size. The image resolution was about 10 mm full width at half maximum at the center. The axial resolution in the direct (cross) plane was about 11 mm (13 mm) full width at half maximum at the center of the field of view.

Calibration between the PET scanner and the well counter was performed for each study with a 10-cm diameter flood phantom filled with ^{68}Ga solution.

The random coincidence and the dead time were corrected with a hardware logic circuit (delayed coincidence) and a software algorithm, respectively.^{19,20} The difference between the corrected true and the ideal true event rates was guaranteed at less than 1% (<5%) up to 50 (80) kcps of the corrected true event rate per slice.^{19,20}

PET Measurement

Each subject was made to lie supine on the couch of the HEADTOME-III with his arms out of the field of view. The imaging position was determined by echocardiography and confirmed by a short-time test transmission scan. A 10-minute transmission scan was made for the attenuation correction with a 3-mCi ^{68}Ge - ^{68}Ga radioactivity ring source of 50 cm in diameter. At 3–4 minutes after a 1-minute C^{15}O inhalation (30 mCi), a 2-minute emission scan was initiated for imaging the distribution of C^{15}O -labeled red blood cells, which was confined to the vascular space. At the start and the end time of the C^{15}O scan, arterial blood was sampled to scale the blood-volume image.

An intravenous injection of 15 mCi H_2^{15}O in 5 ml saline into the antecubital vein was commenced within 2–3 seconds and was followed immediately by a 10-ml saline injection to sweep out the radio-

TABLE 1. Coronary Angiographic Findings

Subject	Study no.	Diagnosis	RCA (%)	Stenosis in LAD (%)			Intervals	
				Seg 6	Seg 7	LCx (%)	Onset to PET	CAG to PET
S1	580	Subnormal (AP)	0	0	0	0		41 days
S2	634	Subnormal (AP)	0	0	0	0		16 days
S3	672	Subnormal (AP)	0	0	0	0		85 days
P1	582	AP	75	75	75	75		43 days
P2	636	AP	75	75	0	90		12 days
P3	685	MI	90	75	75	90	45 days	5 days
P4	728	MI	0	75	75	0	27 years	38 days
P5	730	MI	0	90	0	0	79 days	41 days
P6	734	AP	0	0	99	0		15 days
P7	753	MI	0	99	100	0	117 days	58 days
P8	777	MI	0	0	0	99	64 days	7 days

RCA, right coronary artery; LAD, left anterior descending branch of the left coronary artery; seg 6, segment 6 of LAD; seg 7, segment 7 of LAD; LCx, left circumflex branch of the left coronary artery; PET, positron-emission tomography; CAG, coronary angiography; AP, angina pectoris; MI, myocardial infarction.

activity staining in the vein. The dynamic PET scan was started simultaneously with the H₂¹⁵O injection. The scan sequence consisted of 12 5-second and eight 15-second scans (total, 3 minutes).

Measurement of Input Function

In the H₂¹⁵O dynamic measurements, the input function was obtained by continuously measuring the radioactivity in the arterial blood. Arterial blood was continuously withdrawn during the H₂¹⁵O scan from the femoral artery (N3, S1–S3, and P1–P7) or the radial artery (N1, N2, N4, and P8) at a withdrawal speed of 10 ml/min. The manometer tube (0.5 mm i.d.) and catheter were connected directly without a three-way tap to minimize the dispersion occurring in the tube system. The radioactivity in the blood was monitored by beta-ray detection with a plastic scintillator. The sampling interval was 0.5 seconds. The tube was coiled to about 2 cm in diameter at a distance of about 15 cm from the catheter and was taped onto the beta-ray detector. The dispersion time constant of this tube-detector system was less than 1 second when the dispersion was approximated by a single exponential function.¹⁷

To evaluate and correct for the internal dispersion occurring in the arterial lines, the measured arterial curves were compared with the left ventricle (LV) time-activity curve in sequential H₂¹⁵O images for each study. A systematic discrepancy (dispersion) could be observed in the arterial curves when sampled from the radial artery and even when sampled from the femoral artery in patients with low cardiac output. Such dispersion was corrected by deconvoluting the measured arterial curve by the single-exponential function. Here, the time constant of the single-exponential function was determined so that the deconvoluted curve fit the LV time-activity curve.

The timing discrepancy between the arterial curve and the PET data, which was related to the delay in the arterial lines and in the detector tube, was adjusted absolutely by comparing the arterial curve with the LV curve.

Calibration of the radioactivity sensitivity between the beta-ray detector and the well counter was performed after each study by filling the tube with H₂¹⁵O saline and by counting the same solution in the well counter.

The beta-ray detector was shielded by a 5-cm thick cylindrical-lead container, and the discrimination was set at the level to reject gamma rays.^{17,21} The background count was negligibly small in the measurement of the H₂¹⁵O radioactivity in the blood.

Correction for Blood Volume

Because the red blood cells labeled with C¹⁵O were confined to the vascular space, the C¹⁵O scan provided the blood-volume image, BV(x,y):

$$BV(x,y) = [C^{15}O](x,y)/[C^{15}O]_{well} \quad (8)$$

where [C¹⁵O](x,y) and [C¹⁵O]_{well} represent the C¹⁵O radioactivity concentration of both the PET measurement and the blood sample, respectively. A fraction of the H₂¹⁵O radioactivity in the blood component was removed from the H₂¹⁵O raw image by subtracting the blood-volume image multiplied by arterial concentration of H₂¹⁵O. The net H₂¹⁵O radioactivity in the myocardium, [H₂¹⁵O]_j^{myo}(x,y), was calculated as

$$[H_2^{15}O]_j^{myo}(x,y) = [H_2^{15}O]_j(x,y) - \int_{T_j^i}^{T_j^f} Ca(t)dt * BV(x,y) \quad (9)$$

where [H₂¹⁵O]_j(x,y) is the raw H₂¹⁵O radioactivity in the jth scan at the location (x,y), Ca(t) is the arterial concentration curve, and T_jⁱ and T_j^f are the scan start and stop times of the jth scan, respectively.

Data Analysis

First, the serial images of H₂¹⁵O in the myocardium, [H₂¹⁵O]_j^{myo}(x,y), were accumulated with weighting according to each scan period because the serial images of the HEADTOME-III were already normalized for the scan period.

$$[H_2^{15}O]^{myo}(x,y,T) = \frac{1}{T} \sum_{j=1}^N (T_j^f - T_j^i) [H_2^{15}O]_j^{myo}(x,y) \quad (10)$$

where [H₂¹⁵O](x,y,T) is the integration of the H₂¹⁵O radioactivity from 0 to T at the location (x,y), and N is the number of scans accumulated. T is the scan stop time of the final scan (3 minutes). Second, the MBF images were calculated with the [H₂¹⁵O]_j^{myo}(x,y,T) and the Ca(t) data according to the conventional autoradiographic method (described above).

ROIs were set in three regions of the myocardium (the septum, the anterior wall, and the lateral wall) by referring the autoradiographic MBF image according to the segmentation by Schelbert and coworkers.²² Relatively large ROIs, 2–6-cm diameter ellipse, were adopted to reduce the statistical noise. The total number of the pixels in ROIs was more than 100. The H₂¹⁵O time activity curves, [H₂¹⁵O]_j^{myo}, were obtained for these ROIs. By performing kinetic analysis of the dynamic data, the absolute MBF values and the tissue fractions were calculated for these specified ROIs.

In the present least-squares fitting procedure, the following index (χ^2) was minimized.

$$\chi^2 = \frac{1}{N} \sum_{j=1}^N \frac{\left| \int_{T_j^i}^{T_j^f} Dm(t)dt - [H_2^{15}O]_j^{myo} \right|^2}{|\Delta_j|^2} \quad (11)$$

The values of the weighting factor, $|\Delta_j|^2$, were chosen to correspond to the errors of measurement expected in the jth data. This was intended to normalize each square sum of the numerator in Equation 11 by its accuracy of measurement since

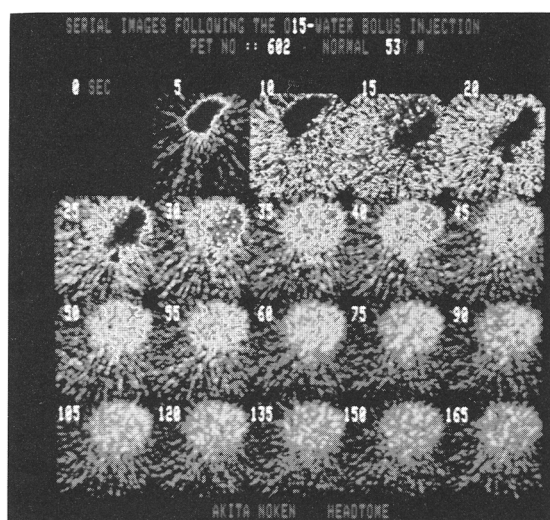
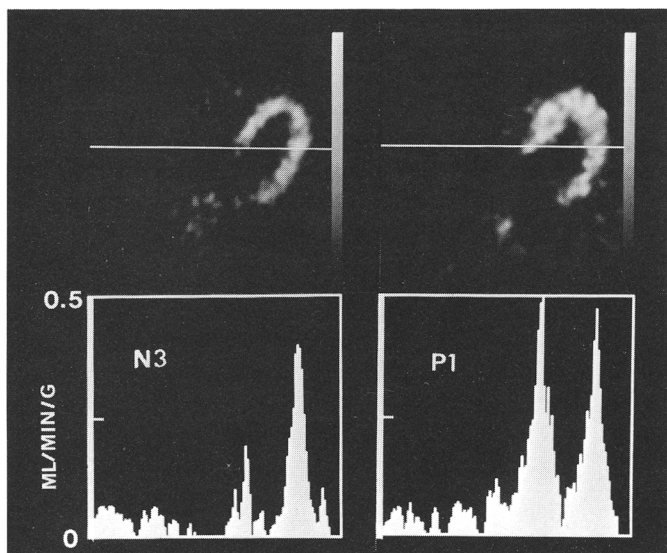


FIGURE 2. *Serial images of the middle of five slices taken from a normal subject after intravenous bolus injection of $H_2^{15}O$. Radioactivity passes through the right ventricle, lung, and left ventricle and diffuses to the myocardium.*

the measurement of each serial image had its own accuracy depending on the period. Thus, the fitting was performed with larger weights for data in which less error was expected and vice versa (see also "Discussion").

Results

The coronary angiographic findings are summarized in Table 1. All subnormal subjects (S1-S3) had negative angiographic indication. Patients P1-P3 had severe stenosis in their main three vessels (triple-vessel disease). Patients P4-P7 had stenosis in the left anterior descending branch of the left coronary artery (LAD). Patient P8 had stenosis in the left circumflex branch of the left coronary artery (LCx).



A typical example of serial images of the middle of the five slices after $H_2^{15}O$ injection is shown in Figure 2. It can be seen that the radioactivity passes serially through the right ventricle (RV), lung, and LV and diffuses to the myocardium.

Figure 3 shows typically obtained autoradiographic MBF images for a normal volunteer (N3) and a patient (P1) together with their profiles. For these calculations, a value of $p=0.91$ ml/g was assumed (see "Discussion"). The autoradiographic MBF values calculated in the lateral wall of N3, whose ROI is depicted in Figure 4A, are plotted in Figure 4B as a function of the accumulation time (T). For $\alpha=1$ g/ml, the autoradiographic MBF values decreased with lengthening accumulation time. On the other hand, the calculated MBF values were independent of the accumulation time for $\alpha=0.55$ ml/g, which was the value obtained by kinetic analysis for the same ROI as described below.

Figure 5 gives a typical example of the radioactivity curve in the lateral wall of N3 (the same region as in Figure 4A). The histogram shows the measured data, and the solid line plots the theoretical prediction best fitted to the measured data. Such curves were already corrected for blood-volume contamination and for radioactive decay. Two parameters (MBF and tissue fraction) were optimized by fitting these two curves. The parameters obtained were $\alpha=0.55$ g/ml and $f=0.97$ ml/min/g, where $p=0.91$ ml/g and $E=1$ were assumed.

The tissue fraction and MBF values were calculated for the same myocardium (lateral wall in N3) but with different sizes of the ROI as shown in Figure 6A. The results are plotted in Figure 6B as a function of the diameter, x , of the ROI. The calculated MBF values revealed no significant changes. On the other hand, the calculated tissue fractions were reasonably decreased with increasing ROI diameter.

FIGURE 3. *Autoradiographic images of myocardial blood flow and their profiles (inset) for normal volunteer (N3) and patient with triple-vessel disease (P1). Note, the vertical scale of both profiles was the same. Myocardial wall in P1 was relatively thick compared with that of N3, which caused a higher flow in patient P1 than in subject N3.*

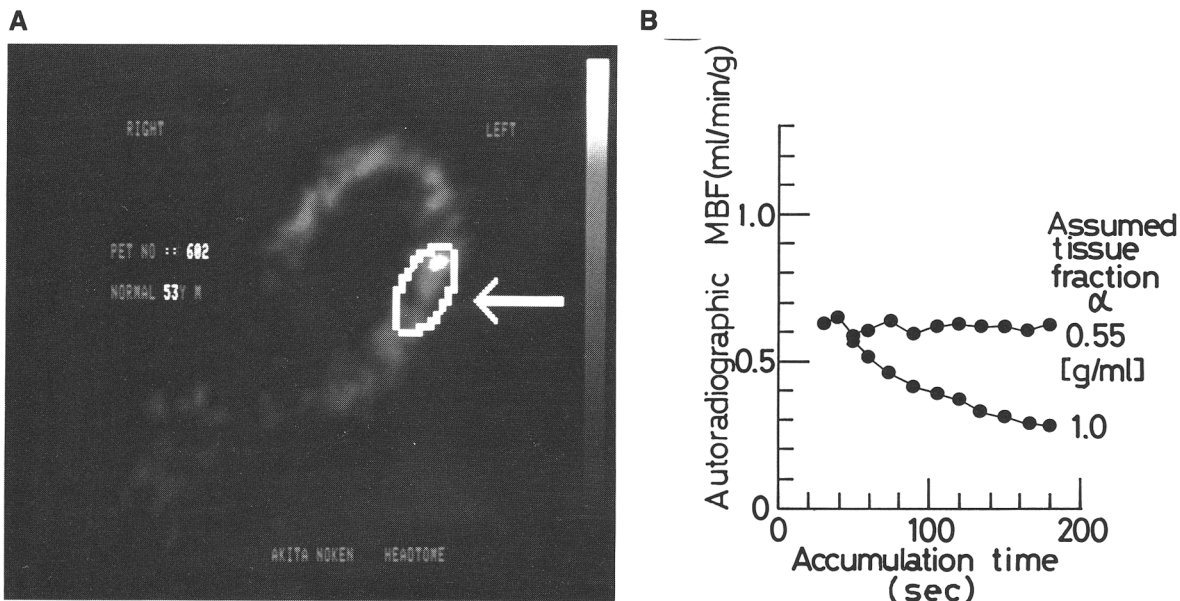


FIGURE 4. Autoradiographic myocardial blood flow (MBF) image of normal volunteer N3 and its region of interest used in analysis (Panel A). Graph of autoradiographic MBF in region of interest as a function of the accumulation time (Panel B). Upper and lower lines were calculated by assuming the tissue fraction as $\alpha=1$ and 0.55 g/ml , respectively. ($\alpha=0.55\text{ g/ml}$ was the value obtained by kinetic analysis as shown in Figure 5.) For $\alpha=1\text{ g/ml}$, the obtained MBF value was decreased when lengthening the accumulation time.

The MBF values obtained by the present kinetic method in normal volunteers and subnormal subjects are summarized in Table 2 for the three regions of the myocardium (the septum, anterior wall, and lateral wall). The averaged MBF values over the three regions in four normal and in three subnormal subjects were 0.97 ± 0.07 and $0.91 \pm 0.10\text{ ml/min/g}$, respectively. The overall mean MBF for the seven subjects was $0.95 \pm 0.09\text{ ml/min/g}$. The

results for the patients are summarized in Table 3. The MBFs were homogeneously decreased in the patients with triple-vessel disease. The mean value ($0.55 \pm 0.09\text{ ml/min/g}$) represented about a 40% decrease relative to the normal subjects. In the patients with stenosis of the LAD, a systematic decrease of MBF was observed in the septum and/or anterior-wall regions. In the patient with stenosis of the LCx, about a 20% decrease was noted in the lateral-wall region. The averaged MBF for the three regions of all the patients was $0.63 \pm 0.26\text{ ml/min/g}$.

Discussion

Introduction of Tissue Fraction

For the purposes of accurate detection and evaluation of cardiac pathophysiology in humans, it is necessary to measure the absolute value of the MBF noninvasively. However, the PVE, which arises from the limited spatial resolution of the scanner and the cardiac wall motion, impairs the quantification of the measurement. This problem is related to a confusion between two different concepts, the tissue concentration and the ROI (spatial) concentration. Kety's model^{8,9} has been commonly used for estimating regional blood flow by PET. This model requires measurement of the tissue concentration, that is, the tracer amount per mass of tissue (Cm, $\mu\text{Ci/g}$). However, the PET method provides the tracer concentration in a specified ROI volume (Dm, $\mu\text{Ci/ml}$). The difference between Cm and Dm sometimes becomes large, especially in cardiac studies. The effect of this difference is not straightforward in the calculation of MBF because of the nonlinear relation between MBF

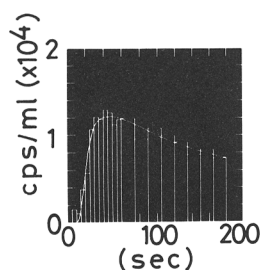


FIGURE 5. Typical tissue radioactivity curve of the myocardium in the lateral wall of a normal volunteer (N3). Region of interest was the same as shown in Figure 4A. Histogram corresponds to the tissue curve measured by positron-emission tomography. Data were relatively noise free compared with those of single pixel of the raw image because the statistical noises were suppressed by averaging whole pixels in the region of interest. Solid line indicates the theoretical prediction obtained by the present kinetic analysis (Equation 7 in the text). Best fit was obtained for $f=0.97\text{ ml/min/g}$ and $\alpha=0.55\text{ g/ml}$. Curves were already corrected for blood-volume contamination and for radioactive decay of ¹⁵O.

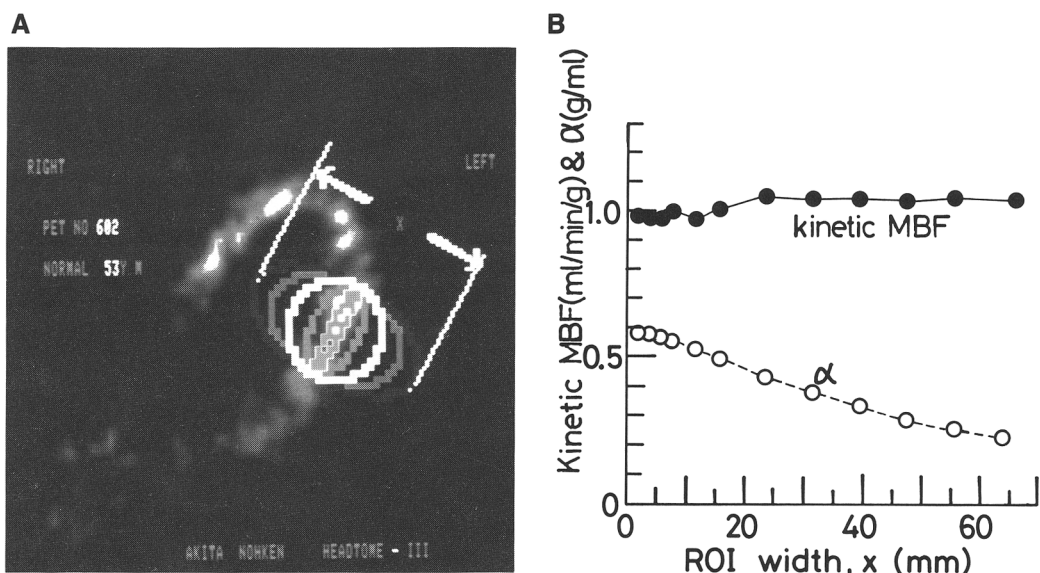


FIGURE 6. Various regions of interest (ROIs) in the myocardium of a normal volunteer (N3) (Panel A). Myocardial blood flows (MBFs) were calculated according to the present kinetic method for these ROIs. ROI size dependence of the calculated MBF and α obtained by the kinetic method (Panel B). The calculations were made for ROIs indicated in left panel. Calculated MBF values revealed no significant changes, while the calculated tissue fractions were decreased with increasing ROI size.

and D_m (or C_m). The concept of the tissue fraction was therefore introduced in the present model as illustrated in Figure 1.

The tissue fraction can be solved by the kinetic method developed in the present study, which was based on $H_2^{15}O$ dynamic measurements. This kinetic method, formulated according to the new model, allowed determinations of two parameters (the regional MBF and the tissue fraction in the specified ROI) to be made under the assumption that the partition coefficient and the extraction fraction were given. Thus, the absolute regional MBF, which was free from the PVE, could be obtained. Moreover, it is possible that the tissue fraction could be used for quantification in measurement of other physiological functions such as glucose utilization and oxygen consumption in PET.

As shown in Figure 6, the MBF values obtained were independent of the size of the ROIs and were almost consistent. On the other hand, the tissue fraction was reasonably decreased with increasing ROI size. These results provide evidence to suggest the validity of the mathematical procedures presented in this paper.

Accuracy of Positron-Emission Tomography

Because, in general, quantification of PET measurement tends to suffer from high-dose radioactivity in the field of view, we need to consider the accuracy of measurements under the high count rates obtained after passage of the RV after intravenous bolus injection of $H_2^{15}O$. In the HEADTOME-III, the measured events were corrected for random coincidence and dead time. The

difference between the corrected true and the ideal true event rate was guaranteed at less than 1% (<5%) up to 50 (80) kcps of the corrected true event rate per slice.²⁰ Because the maximum counting rate was 50–80 kcps at the peak after the injection for the typical injection dose of 15 mCi, the true $H_2^{15}O$ distribution in the field of view would be measured with an accuracy of less than 5% at maximum.

The accuracy of this measurement was checked by comparing the LV time-activity curve with the arterial curve in the $H_2^{15}O$ measurements. The LV:blood ratio in the $C^{15}O$ measurement was 0.94 ± 0.06 for 15 subjects. The decrease of about 6% would result from spillover of the LV radioactivity because of the PVE. In the $H_2^{15}O$ studies, when the injection dose was less than 20 mCi, the ratio of the first 60-second integration of the $H_2^{15}O$ LV curve to that of the arterial curve was almost equal to the LV:blood ratio in the $C^{15}O$ measurement within 10% fluctuation. As shown in Figure 7, which illustrates one of our early studies with an injection dose of 20 mCi, good agreement was seen between the two curves. Thus, the measurements should be sufficiently accurate in terms of the dead-time effect because 15 mCi $H_2^{15}O$ was typically injected in the present study.

One might consider possibility of a noninvasive study with the use of the LV curve as the input function. However, the present kinetic calculation would require very accurate measurement of the input function. The 6% spillover of the LV radioactivity could not be neglected. Our simulation study demonstrated that the 6% decrease around the peak

TABLE 2. Myocardial Blood Flow in Normal and Coronary Angiographic Normal Subjects

Subject	Study no.	Age (years)	Sex	Hct	Septum	Myocardial blood flow (ml/min/g)		Combined mean and SD
						Anterior wall	Lateral wall	
N1	477	30	M	0.48	1.00	0.95	0.98	
N2	515	25	M	0.44	1.05	1.00	1.07	
N3	602	53	M	0.42	0.85	0.99	0.97	
N4	848	53	M	0.43	0.82	1.03	0.97	
Mean					0.93	0.99	1.00	0.97
SD					0.11	0.03	0.05	0.07
S1	580	53	M	0.43	0.93	0.94	0.96	
S2	634	59	F	0.35	0.80	1.08	1.02	
S3	672	54	M	0.40	0.80	0.79	0.88	
Mean					0.84	0.94	0.95	0.91
SD					0.08	0.15	0.07	0.10
Combined N1-S3						0.89	0.96	0.95
Mean						0.09	0.09	0.09
SD								

Hct, hematocrit; N, normal subject; S, subnormal subject.

of the input function produced systematic errors of a few tens of percentage in calculated values for MBF and α . We, therefore, obtained the input function by measuring the arterial concentration curve, minimizing the dispersion and the ambiguity of the time delay for all studies.

Measurement of Input Function

As described by us recently,^{17,21} accurate measurement of the input function was important for measuring the quantitative blood flow by the autoradiographic method. The degree of dispersion in the present system was substantially improved compared with the previous one.^{17,21} A thinner tube (0.5 mm i.d.) was used; the withdrawal speed was sufficiently high (10 ml/min); and the tube was directly connected to the catheter without a three-way tap. Moreover, the deconvolution of the measured arterial curve, which was performed only for subjects having a significantly large internal dispersion, increases the accuracy of measurement of the true input function even for patients with very high internal dispersion due to low output.

Comparison of the arterial curves with the LV curves has another advantage in improving the ambiguity of the absolute time axis of the measured arterial curves. The time axis of the measured arterial curve was adjusted to the time axis of the PET measurement. The accuracy of this adjustment technique, which might be within $\pm 1\text{--}2$ seconds, would be much better than in other studies.^{4\text{--}6}

Autoradiographic Myocardial Blood Flow

The present method for calculating the MBF image was based on a conventional theory of the H₂¹⁵O autoradiographic technique,^{13\text{--}17} which Bergmann et al⁴ first applied to the cardiac PET study.

The following aspects were improved in the present study. The input function was accurately obtained. That is, arterial radioactivity was continuously monitored with a 0.5-second sampling interval; time delay of the arterial curve was adjusted to absolute time axis of PET data analysis by comparing the arterial curve with the LV time activity curve; and the net dispersion was negligibly small or corrected by a deconvolution technique. The blood-volume contamination was corrected absolutely by measurement of the blood radioactivity concentration in the C¹⁵O and H₂¹⁵O scans as shown in Equation 9. A scanner with high-counting rate characteristics was used.^{19,20}

As shown in Figure 3, the MBF image was calculated from the autoradiographic data. It may be helpful for gaining an insight into the blood flow distribution intuitively. However, autoradiographic MBF obtained in this manner would be systematically lower than the true value. It is demonstrated intuitively in Figure 3, where the profiles were not flat at the peak, suggesting a limited spatial resolution of the measurement. When we performed ROI analysis, the averaged MBF value in the specified ROI must have depended on the size of the ROI. Also, the peak height must have depended on the wall thickness and wall motion. As can be seen from Figure 3, higher flow values were yielded by the autoradiographic method for patient P1 than for subject N3, although patient P1 was confirmed as having severe stenosis in his main three vessels by coronary angiography. This spurious result would be due to his relatively thick-walled myocardium. Indeed, the kinetic analysis, as described above, proved that the MBF in patient P1 was uniformly low.

We fixed the tissue fraction at 1 g/ml when calculating the autoradiographic MBF image in this paper. The true value is certainly smaller than this in

TABLE 3. Myocardial Blood Flow in Patients and Subjects

Subject	Study no.	Age (years)	Sex	Hct	Septum	Myocardial blood flow (ml/min/g)		
						Anterior wall	Lateral wall	Combined mean and SD
P1	582	67	M	0.45	0.48	0.57	0.59	
P2	636	50	M	0.44	0.58	0.58	0.59	
P3	685	62	F	0.36	0.34	0.54	0.67	
Mean					0.47	0.56	0.62	0.550
SD					0.10	0.02	0.03	0.09
P4	728	45	M	0.40	0.31	0.15	0.66	
P5	730	57	M	0.39	0.28	0.76	1.12	
P6	734	60	F	0.36	0.78	0.71	0.79	
P7	753	65	M	0.41	0.44	0.25	0.99	
Mean					0.45	0.47	0.89	0.60
SD					0.20	0.27	0.18	0.30
P8	777	66	M	0.30	0.96	1.10	0.77	
Combined P1-P8					0.52	0.58	0.77	0.63
Mean					0.22	0.28	0.18	0.25

Hct, hematocrit; P1-P3, patients with triple-vessel disease; P4-P7, patients with left anterior descending coronary artery stenosis; P8, patients with left circumflex stenosis (see also Table 1).

cardiac studies because of the PVE. This choice of tissue fraction thus produced a systematic underestimation of the MBF. The calculated MBF was, moreover, dependent on the accumulation time as shown in Figure 4B. (The calculated value decreased with lengthening of the accumulation time.) The correct value of the tissue fraction must therefore be used for each pixel when we need to calculate the quantitative and time-independent MBF image, although there is no way of determining the tissue fraction in the autoradiographic approach.

Kinetic Myocardial Blood Flow

The regional MBF was calculated for three myocardial segments (the septum, anterior wall, and lateral wall) in each subject according to the kinetic method. The present kinetic method enabled us to obtain absolute MBF values for each ROI. Also, the tissue fraction could be determined. Note that the tissue fraction included two concepts, that is, the spillover effect due to the limited spatial resolution of PET and the myocardial wall movement throughout the ROI. The obtained MBF was free from the PVE. As shown in Table 2, the MBFs for the normal and subnormal groups revealed a relatively small difference among the subjects and were almost consistent in the three regions. The averaged MBFs for the normal and subnormal groups were 0.97 ± 0.07 and 0.91 ± 0.10 ml/min/g, respectively. On the other hand, in the patients, the MBFs were significantly reduced and showed larger deviations compared with the normal subjects (Table 3).

In the subnormal subjects, coronary angiography detected no abnormalities. Moreover, no significant uptake of ^{18}F -fluoro-deoxyglucose was observed in their myocardium during a study in the fasted

condition. These findings suggest that they had no ischemic state in the myocardium in the resting condition. This is consistent with our observation of no significant decrease in calculated MBF from the value of normal volunteers.

In the patients with triple-vessel disease, the MBFs were diffusely reduced (Table 3). The averaged MBF showed about a 40% decrease relative to the normal subjects with a standard deviation of 16%. This homogenous decrease may be consistent with their coronary angiographic findings (see also Table 1) as well as the global uptake of ^{18}F -fluoro-deoxyglucose in their myocardium in the fasted condition (about 9 hours after a meal).²³ The kinetic method presented here could thus detect such a homogenous decrease of the MBF in triple-vessel disease, although the conventional autoradiographic method failed to demonstrate any abnormality as typically shown in Figure 3.

In the patients with stenosis in the LAD (in segment 6 and/or 7), the MBFs were significantly decreased in the septum and/or anterior wall, rather than in the lateral wall. In patient P8 who had stenosis only in the LCx, the MBF in the lateral wall was slightly reduced compared with the other regions, and the MBFs in the septum and anterior wall were within the normal range. These observations seemed to be consistent, although anatomic correspondence of each segment to ROI in PET might not be proved. It is of interest to examine the precise correlation between the degree of stenosis and absolute value of MBF in its dominant region. However, this is beyond the scope of present study. Further investigations are in progress on a larger number of subjects and will be published elsewhere (in preparation).

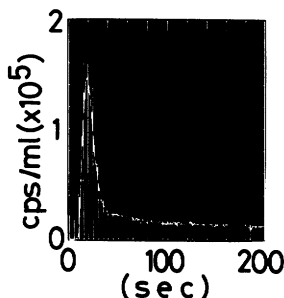


FIGURE 7. Typical comparison of the arterial radioactivity curve (solid line) with the left ventricle (LV) radioactivity curve (histogram) after intravenous bolus injection of 20 mCi H₂¹⁵O. LV curve was already multiplied by a spillover correction factor, that is, inverse of the LV:blood ratio obtained in C¹⁵O measurement ($\approx 1/0.93$ in this case).

The MBF values in the normal subjects (all were studied in the resting condition) showed a relatively low interindividual variability compared with other techniques (e.g., the ¹³³Xe clearance method). The standard deviations were 7.6% for normal, 10.7% for subnormal, and 9.3% for all subjects combined (i.e., normal and subnormal). This indicates stability of the present method, although our analysis was based on a relatively small number of subjects.

Fitting Procedure

The introduction of the weight in Equation 11 was important in the fitting procedure of the kinetic analysis since each of the scan data has a different accuracy of measurement. In the present study, the errors expected in the jth measurement of the myocardial concentration were multiplied inversely in calculating each square sum of Equation 11 so that each square sum was normalized by its expected accuracy. Hence, each square of Equation 11 would have its own significance corresponding to the accuracy of each measurement.

The following five error factors were taken into account: 1) statistical fluctuation of ROI concentration curve, 2) insufficient temporal smoothing of the wall motion, 3) errors of subtraction for the radioactivity in the blood volume, 4) the effect of radioactivity in the lung, and 5) inaccuracy of the scanner itself.

As for the first factor, the statistical noise was derived as an inverse of a square root of each ROI concentration data.

Regarding the second factor, we assumed that the wall movement through the ROI was completely smoothed during each scan period. However, a 5-second scan may not be sufficient for complete smoothing. For a typical heart rate of 60 beats/min, about 10% of this error would be expected at maximum in the 5-second measurement. Thus, this error would be proportional to the inverse of each scan period.

The error of the blood-volume subtraction was large at the early phase near the LV peak and became small at the later phase. To cancel out the error of the blood-volume subtraction, the LV concentration data that would be almost equal to the subtraction level were multiplied inversely as one of the weights in calculating the square sum of Equation 11. Further, the data before the appearance of H₂¹⁵O radioactivity in the LV were neglected since the H₂¹⁵O will not exist in the myocardium before then. Thus, the time difference of the H₂¹⁵O radioactivity in the RV and LV was almost negligible in the calculation for the septum region.

Regarding the H₂¹⁵O radioactivity in the lung, the blood volume of the lung is not negligible, although the lung tissue H₂¹⁵O would be small compared with that in the myocardium. Therefore, subtraction of the blood volume may produce a large error due to the difference in the appearance time of H₂¹⁵O in the lung and in the LV. To cancel out this subtraction error in addition to the effect of the lung tissue radioactivity itself, we used the concentration curve in a typical lung region as the weight corresponding to the fourth term.

Concerning the fifth factor, the inaccuracy of the scanner was estimated on the basis of previous studies^{19,24,25} and phantom experiments.¹⁷

Thus, $|\Delta_j|^2$ was determined as

$$\begin{aligned} |\Delta_j|^2 &= \sum_{i=1}^5 |\Delta_j^i|^2, \\ |\Delta_j^1|^2 &= W_1 / [H_2^{15}O]_{j,ROI}^{ROI}, \\ |\Delta_j^2|^2 &= W_2 / (T_j^f - T_j^i) \\ |\Delta_j^3|^2 &= W_3 [H_2^{15}O]_{j,LV}^{LV} \\ |\Delta_j^4|^2 &= W_4 [H_2^{15}O]_{j,LUNG}^{LUNG} \\ |\Delta_j^5|^2 &= W_5 \end{aligned} \quad (12)$$

where the superscripts ROI, LV, and LUNG represent the radioactivity in the myocardial ROI, in the LV, and in the lung, respectively.

As a result of these procedures, the early phase data were almost neglected in the calculation (due mainly to the third and fourth factors) because the weight (inverse of $|\Delta_j|^2$) was small at the early phase near the peaks of the RV, the lung, and the LV. It is of importance, therefore, that the optimization of the kinetic parameters be made mainly by weighting the absolute height and the shape of the H₂¹⁵O myocardium concentration curve at the decreasing slope. This supposes that flow determination becomes inaccurate in either extreme range of low flow (MBF≈0) or high flow (MBF≈∞) as explained in the following. As MBF decreases, height of tissue curve is reduced; hence, relatively large contamination of surrounding tissue occurs. This is essentially the same effect as a conventional clearance technique. On the other hand, as MBF extremely increases, the tissue curve becomes sharp

as it approaches the arterial curve, and its early portion is rendered to be neglected where most of flow information is included.

H₂¹⁵O as Myocardial Blood Flow Tracer

The present method was based on the following assumptions concerning the suitability of the tracer used. 1) H₂¹⁵O is ideally permeable across the capillary membrane (single-pass extraction fraction is unity, E=1). 2) The tracer is diffusible in the tissue space, and the distribution reaches equilibrium instantaneously. 3) The tissue/blood partition coefficient, p (ml/g), can be fixed.

Concerning the first assumption, any diffusible tracer theoretically has a limitation of permeability across the capillary membrane. Using Crone's model,²⁶ the single-pass extraction fraction, E, can be expressed as

$$E = 1 - e^{-PS/f} \quad (13)$$

where PS (ml/min/g) is the product of the capillary permeability and surface area. Therefore, E becomes reduced (E<1) for finite PS. However, as for the use of H₂¹⁵O, this represented a minor factor in the myocardium as reported by Bergmann et al.⁴ They estimated the extraction fraction for H₂¹⁵O in the dog myocardium 0.96±0.05 in the flow range of 0.8–1 ml/min/g. This higher extraction in the myocardium compared with the brain tissue might be due to greater capillary density (larger S) in the myocardium.

As for the second assumption, the diffusion speed was precisely calculated for tissues with normal capillary density and seemed to be sufficiently high in the current time scale.^{8,9,25,27}

The final assumption involves two parts. The first is related to the definition of p (or adequacy of model assumed), and the second is related to the uncertainty of choice of p for each individual. In the present study, the tissue/blood partition coefficient is defined as the ratio of the water content in the tissue to that in the blood. This is based on the assumption that all tissue water is freely exchangeable. However, some investigators have proposed a limitation to this assumption in view of their observations; that is, the water distribution volume in the brain tissues obtained by their method was significantly smaller than the predicted value²⁸ and was dependent on the measurement time.²⁹ Their findings suggest the possible existence of a considerable amount of a slowly exchanging component in the tissue water. On the contrary, their results could have been derived from neglected errors with respect to the measurement of the input functions (dispersion and time shift) as well as the tissue heterogeneity. We recently estimated the water distribution volume of the brain tissue with a highly accurate measurement system. Our preliminary data revealed no evidence that suggested a considerable amount of a slowly exchanging component in the tissue

water.³⁰ Thus, the first part of this assumption seems to be reasonable for the present study.

The second part of the final assumption (variation of p) concerns the variation of water content in the myocardium and blood in each individual. Uncertainty of p should directly affect the errors in the determination of f and α since f and p are calculated as $f=(k_2 p)/E$ and $\alpha=(k_1/k_2)p$, respectively. This error might become important in the evaluation of ischemic lesions or necrotic tissues. Further consideration is needed with regard to this point.

Acknowledgments

We are greatly indebted to the staff of the Research Institute for Brain and Blood Vessels-Akita, in particular, Messers. Y. Shoji, E. Hagami, T. Hachiya, and Y. Aizawa for their assistance. We wish to thank Ms. Shoko Ishioka for her helpful secretarial work.

References

1. Wisenberg G, Schelbert HR, Hoffman EJ, Phelps ME, Robinson GD, Selin CE, Child J, Skorton D, Kuhl DE: In vivo quantitation of regional myocardial blood flow by positron-emission computed tomography. *Circulation* 1981; 63:1248–1258
2. Henze E, Huang SC, Ratib O, Hoffman E, Phelps ME, Schelbert HR: Measurement of regional tissue and blood radiotracer concentrations from serial tomographic images of the heart. *J Nucl Med* 1983;24:987–996
3. Wilson AR, Shea MJ, De Landsheere CM, Turton D, Brady F, Deanfield JE, Selwyn AP: Validation of quantitation of regional myocardial blood flow in vivo with ¹¹C-labeled human albumin microspheres and positron emission tomography. *Circulation* 1984;70:717–723
4. Bergmann SR, Fox KA, Rand AL, McElvany KD, Welch MJ, Markham J, Sobel BE: Quantification of regional myocardial blood flow in vivo with H₂¹⁵O. *Circulation* 1984;70:724–733
5. Huang SC, Schwaiger M, Carson RE, Carson J, Hansen H, Selin C, Hoffman EJ, MacDonald N, Schelbert HR, Phelps ME: Quantitative measurement of myocardial blood flow with oxygen-15 water and positron computed tomography: An assessment of potential and problems. *J Nucl Med* 1985; 26:616–625
6. Knabb RM, Fox KA, Sobel RE, Bergmann SR: Characterization of the functional significance of subcritical coronary stenoses with H₂¹⁵O and positron-emission tomography. *Circulation* 1985;7:1271–1287
7. Hoffman EJ, Huang SC, Phelps ME: Quantitation in positron emission tomography: 1. Effect of object size. *J Comput Assist Tomogr* 1979;3:299–308
8. Kety SS: The theory and applications of the exchange inert gas at the lung and tissues. *Pharmacol Rev* 1951;3:1–41
9. Kety SS: Measurement of local blood flow by the exchange of an inert, diffusible substance. *Methods Med Res* 1960; 8:228–236
10. Konno O, Simano K: *Biochemical Data*. Tokyo, Igaku-Shoin, 1965, pp 440–441
11. Davis FE, Kenyon K, Kirk J: A rapid titrimetric method for determining the water content of human blood. *Science* 1953;118:276–277
12. Herscovitch P, Raichle ME: What is the correct value for the brain-blood partition coefficient of water? *J Cereb Blood Flow Metab* 1985;5:65–69
13. Kanno I, Lassen NA: Two methods for calculating regional cerebral blood flow from emission computed tomography of inert gas concentrations. *J Comput Assist Tomogr* 1979; 3:71–76

14. Herscovitch P, Markham J, Raichle ME: Brain blood flow measured with intravenous H₂¹⁵O: I. Theory and error analysis. *J Nucl Med* 1983;24:782-789
15. Raichle ME, Martin WRW, Herscovitch P, Mintun MA, Markham J: Brain blood flow measured with intravenous H₂¹⁵O: II. Implementation and validation. *J Nucl Med* 1983; 24:790-798
16. Kanno I, Lammertsma AA, Heather JD, Gibbs JD, Rhodes CG, Clark JC, Jones T: Measurement of cerebral blood flow using bolus inhalation of C¹⁵O₂ and positron emission tomography: Description of the method and its comparison with the C¹⁵O₂ continuous inhalation method. *J Cereb Blood Flow Metab* 1984;4:224-234
17. Iida H, Kanno I, Miura S, Murakami M, Takahashi K, Uemura K: Error analysis of a quantitative cerebral blood flow measurement using H₂¹⁵O autoradiography and positron emission tomography, with respect to the dispersion of the input function. *J Cereb Blood Flow Metab* 1986;6:536-545
18. Hagami E, Murakami M, Takahashi K, Kanno I, Aizawa Y, Hachiya T, Shoji Y, Shishido F, Uemura K: Studies on the direct synthesis of [O-15]-H₂O. *Jpn J Nucl Med* 1986; 23:351-358
19. Kanno I, Miura S, Yamamoto S, Iida H, Murakami M, Takahashi K, Uemura K: Design and evaluation of a positron emission tomograph: Headtome III. *J Comput Assist Tomogr* 1985;9:931-939
20. Yamamoto S, Amano M, Miura S, Iida H, Kanno I: Dead time correction method using random coincidence for PET. *J Nucl Med* 1986;27:1925-1928
21. Kanno I, Iida H, Miura S, Murakami M, Takahashi K, Sasaki H, Inugami A, Shishido F, Uemura K: A system for cerebral blood flow measurement using H₂¹⁵O autoradiographic method and positron emission tomography. *J Cereb Blood Flow Metab* 1987;7:143-153
22. Schelbert HR, Wisenberg G, Phelps ME, Gould KL, Henze E, Hoffman EJ, Gomes A, Kuhl D: Noninvasive assessment of coronary stenoses by myocardial imaging during Pharmacologic Coronary Vasodilation. *Am J Cardiol* 1982; 49:1197-1207
23. Marshall RC, Tillisch JH, Phelps ME, Huang SC, Carson R, Henze E, Schelbert H: Identification and differentiation of resting myocardial ischemia and infarction in man with positron computed tomography, ¹⁸F-labeled fluorodeoxyglucose and ¹³N ammonia. *Circulation* 1983;67:766-778
24. Budinger TF, Derenzo SE, Greenberg WL, Gullberg GT, Huesman RH: Quantitative potentials of dynamic emission computed tomography. *J Nucl Med* 1978;19:309-315
25. Iida H, Kanno I, Miura S, Murakami M, Takahashi K, Uemura K: A quantitative evaluation of blood-brain barrier of brain tumors using ⁶⁸Ga-EDTA and dynamic PET: A proposal of a model considering with finite diffusion speed. Proceedings of international symposium on current and future aspects of cancer diagnosis with positron emission tomography. October 14-18, 1985, Sendai, Japan, pp 220-227
26. Crone C: Permeability by use of the indicator diffusion method. *Acta Physiol Scand* 1963;58:292-305
27. Thews G: Implication to physiology and pathology of oxygen diffusion at the capillary level, in Schade JP, McMenemy WH (eds): *Selective Vulnerability of the Brain*. Oxford, Blackwell, 1963, pp 27-40
28. Huang SC, Carson RE, Hoffman EJ, Carson J, MacDonald N, Barrio JR, Phelps ME: Quantitative measurement of local cerebral blood flow in humans by positron computed tomography and ¹⁵O water. *J Cereb Blood Flow Metab* 1983; 3:141-153
29. Huang SC, Gamhir SS, Hawkins RA, Phelps ME: Investigation of Kety-Schmidt single-compartment model for ¹⁵O water in CBF measurements using PET (abstract). *J Nucl Med* 1983;27:141
30. Iida H, Kanno I, Miura S, Murakami M, Takahashi K, Inugami A, Shishido F, Uemura K: An accurate determination of regional brain/blood partition coefficient of water using dynamic positron emission tomography: Validation of Kety-Schmidt single compartment model for H₂¹⁵O based CBF measurement. *J Cereb Blood Flow Metab* 1987;7(suppl 1):S576

KEY WORDS: • myocardial blood flow • partial volume effect • ¹⁵O-labeled water • positron-emission tomography